Supramolecular chemistry of two new bis(1,2,3-triazolyl)pyridine macrocycles: metal complexation, self–assembly and anion binding

Arthur H. G. David,[a,b†] Rosemary J. Goodwin[a] and Nicholas G. White*[a]

Two new macrocycles containing the bis(1,2,3-triazolyl)pyridine (**btp**) motif were prepared in high yields from a **btp** diazide precursor (**1**). Solution ^{1}H NMR studies show that this diazide undergoes self–assembly with divalent transition metal ions to form ML_2 complexes with pendant azide groups, apparently suitable for conversion into metal-templated catenanes; however attempts to form these catenanes were unsuccessful. Instead a new macrocycle containing two **btp** motifs was prepared, which forms a nanotube structure in the solid state. Reduction of the azide groups to amines followed by amide bond formation was used to convert **1** into macrocycle **8** containing **btp** and isophthalamide functionalities. This macrocycle binds halide and oxalate anions in acetonitrile solely through the isophthalamide motif, and binds aromatic dicarboxylates very strongly through both the isophthalamide amide donors and the **btp** triazole donors. The macrocycle was complexed with Pd(II) and the resulting complexes were shown to bind strongly to halide anions. The solid state structures of these [Pd**8**X]BF_4 (X = Cl^-, Br^-, I^-) were investigated by X-ray crystallography, which showed that [Pd**8**Br] forms an unusual "chain of dimers" structure assembled by metal complexation, N–H–Br^- hydrogen bonding and short Pd–Pd contacts.

Introduction

Macrocycles hold a privileged place within supramolecular chemistry,[1] primarily because their preorganized structures can enhance guest binding through chelate/macrocyclic effects. As the field of supramolecular chemistry has matured, interest has moved from simple macrocycles to larger assemblies of macrocycles. Perhaps most prominent has been the development of intricate interlocked structures such as catenanes and rotaxanes, which contain one or more macrocycles.[2–4] However, other self–assembled structures can be prepared from macrocycles such as dimers,[5–10] tetramers,[11] and hexamers,[12] or nanotube assemblies.[13–18]

Given the prominent role of macrocyclic structures in supramolecular chemistry, the development of new macrocycles is of continuing interest. We were interested in preparing macrocycles incorporating the bis(1,2,3-triazolyl)pyridine (**btp**) motif as the combination of triazole and pyridine *N*-donors and polarized triazole C–H hydrogen bond donors offers the potential for binding of either transition metals, anions, or both.[19,20] Two isomers of the **btp** motif have been commonly studied (Figure 1): the 3,5-**btp** motif has been extensively studied in the context of anion recognition, and derivatives containing an *N*-alkylated pyridinium group and/or halotriazole groups for halogen bonding have proven to be highly effective in this regard.[21–23] The 2,6-**btp** motif has primarily been used for coordination to a wide range of metal ions,[24–33] but has also been used for anion recognition[34–36] and anion binding catalysis[37] (the reader is directed to a recent review for a comprehensive overview of the chemistry of the 2,6-**btp** motif[20]). Interestingly, Byrne and Gunnlaugsson have also demonstrated that the 2,6-**btp** motif can self-recognise through C–H–N hydrogen bonding, and have used this recognition to template the formation of catenanes.[38–40]

We initially targeted macrocycles[34,35] containing the 2,6-**btp** motif as a possible route to catenanes containing both metal and anion binding motifs with the hope that these would be suitable for both anion and metal binding, and potentially also ion pair recognition[41,42] (Figure 2). It was also thought that this approach may allow relatively easy access to catenane oligomers[43–46] such as [3], [5] or [7]catenanes, which are notoriously difficult to prepare.[45] Our planned approach was to use the well-established complexation of two **btp** motifs around a transition metal ion to form a complex with pendant azide groups and then use copper catalysed azide alkyne cycloaddition (CuAAC) reactions with 2,6-diethynylpyridine as the catenane forming reaction (Figure 2). Our attempted catenane synthesis was eventually unsuccessful; however, we instead synthesized two new **btp** macrocycles in high yields. One of these forms nanotubes in the solid state, while the other displays interesting anion and transition metal coordination chemistry in solution and self–assembly in the solid state.

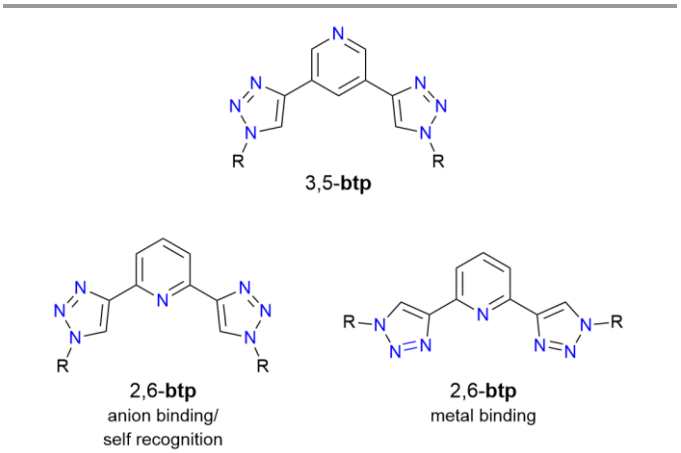

Figure 1 Structures of two isomers of **btp** including both common conformations of the 2,6 isomer. The 3,5 isomer is often functionalised through either *N*-alkylation of the pyridine ring or incorporation of halogen groups at the 5-position of the triazole ring for anion recognition applications

[a] *Research School of Chemistry, Australian National University, Canberra, ACT, Australia. Website: www.nwhitegroup.com. Email: nicholas.white@anu.edu.au.*
[b] *Institut des Sciences Chimiques de Rennes, Université de Rennes 1, 35042, Rennes, France*
† Current address: MOLTECH-Anjou, CNRS, Université d'Angers, 49000 Angers, France
Electronic Supplementary Information (ESI) available: Additional experimental procedures and details, characterisation data.

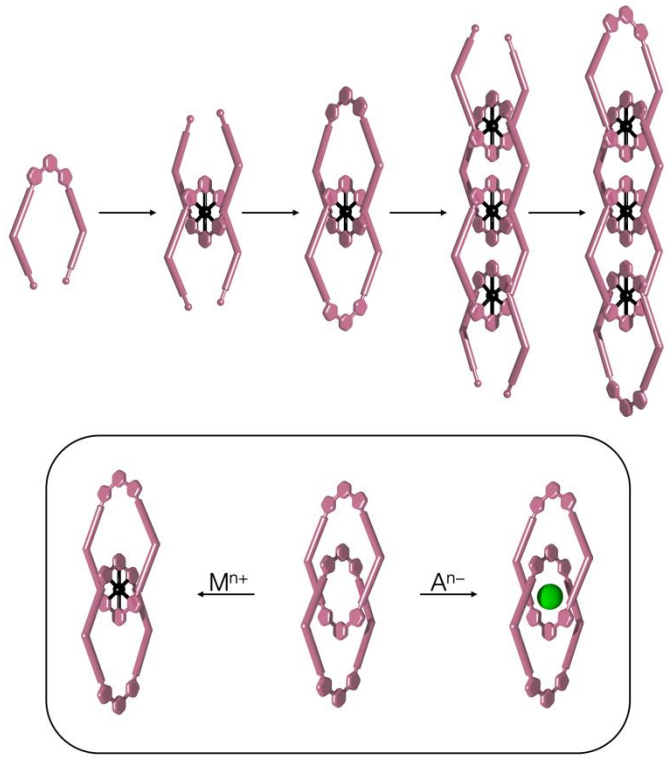

Figure 2 Planned synthesis of **btp**-containing catenanes using a sequence of metalation and CuAAC reactions to generate new **btp** motifs. The inset shows the potential of a resulting catenane to bind metals through bis-terdentate coordination, or anions through C–H-anion hydrogen bonds.

Results and discussion

Synthesis and metal complexation of btp diazide 1

We initially prepared the **btp** diazide **1** by CuAAC of 2,6-diethynylpyridine and a large excess of known diazide **2** (synthesis given in the ESI). We found that using ten equivalents of **2**, *i.e.* five equivalents per alkyne group gave good yields (84%) of **1** after purification by careful column chromatography (Scheme 1).

We then studied the interaction of this compound with transition metal ions, hoping that we would be able to arrange two molecules of **1** around a metal ion and then use subsequent CuAAC reactions to form a [2]catenane.

We studied the complexation of Zn^{2+} *via* ^{1}H NMR titration experiments, using $[Zn(OH_2)_6](ClO_4)_2$ as a Zn^{2+} source with weakly coordinating anions to favour **btp** complexation. When these experiments were conducted in CD_3CN (Figure 3 and Figure S22) or 1:1 $CDCl_3$:CD_3OD (Figure S23), peak shifts consistent with initial formation of the desired ML_2 complex were observed after addition of 0.5 equivalents of Zn^{2+}, followed by conversion to a ML complex with further addition of metal ion.

The ML_2 complex shows upfield shifts of the hydroquinone and CH_2 groups, consistent with these stacking around the Zn-**btp** motifs. These signals then shift downfield upon conversion to the ML complex, which we attribute to the subsequent loss of these stacking interactions. Interestingly in CD_3CN, free ligand and the ML_2 complex are in fast exchange on the ^{1}H NMR timescale, while the ML_2 and ML complex are in slow exchange (Figure 3). In 1:1 $CDCl_3$:CD_3OD, similar peak movements are evident, but all species are in fast exchange on the NMR timescale. When complexation experiments were conducted in d_6-DMSO, no evidence for complexation was observed (Figure S24), suggesting that the **btp** ligand is not able to out-compete this coordinating solvent.

It is notable that some ML_2 species is present even when 5.0 equivalents of Zn^{2+} have been added, and generally the ^{1}H NMR data are consistent with an ML_2 species being the predominant form in solution when 0.5 equivalents of Zn^{2+} are present. When **1** was crystallised from 1:1 chloroform:methanol in the presence of either 0.5 or 1.0 equivalents of Zn^{2+}, we obtained single crystals. We attempted numerous data collections on these crystals using either a home source X-ray diffractometer or synchrotron radiation. For all datasets, data quality were so poor that the structure could not be refined, although it is clear in all cases that the crystals are of the ML_2 complexes (see ESI for full details).

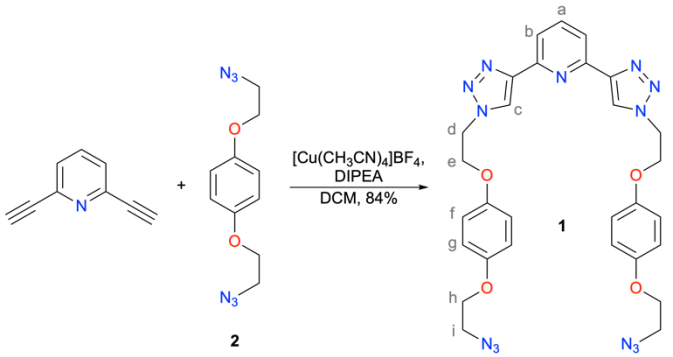

Scheme 1 Synthesis of diazide **1**.

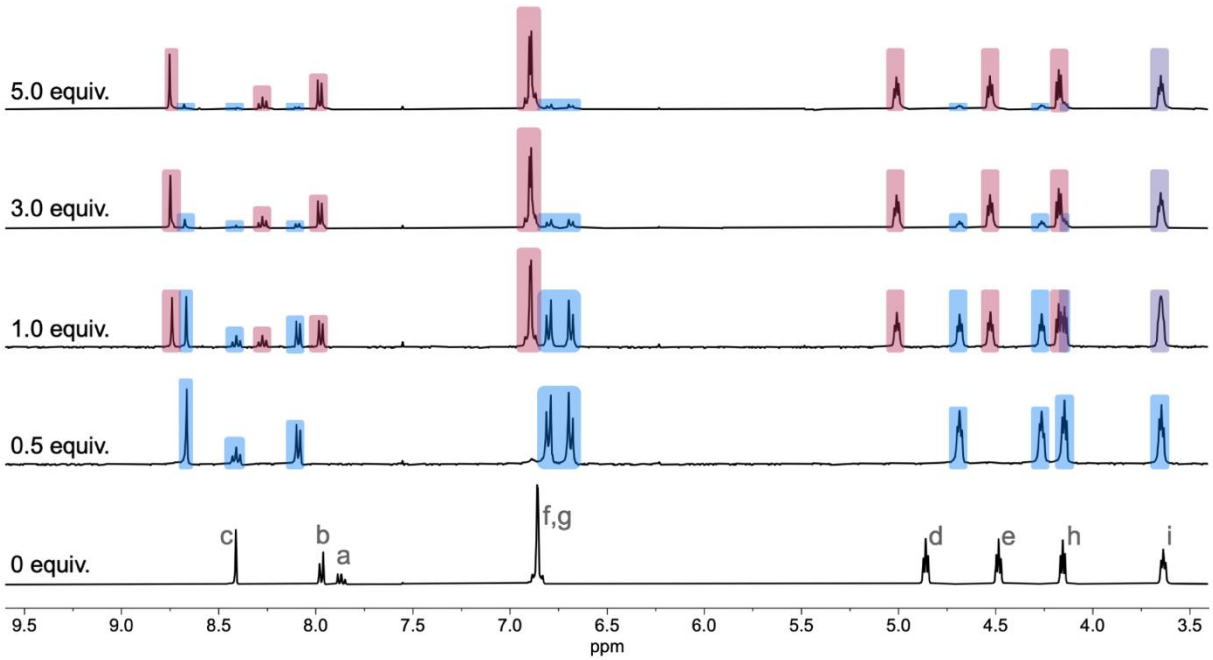

Figure 3 Partial ^{1}H NMR spectra of diazide **1** upon addition of $[Zn(OH_2)_6](ClO_4)_2$. Peak labelling corresponds to atom labelling shown in Scheme 1. Peaks assigned to the ML_2 species are coloured blue, peaks assigned to the ML species are coloured maroon. An expanded version of this Figure including additional equivalents of Zn^{2+} is provided as Figure S22 (2.0 mM **1** in CD_3CN, 400 MHz, 298 K).

Attempts to form [2]catenanes from ML_2 complexes of 1

Given the robust formation of ML_2 complexes with **1**, we next attempted to use these complexes to form metallocatenanes by reacting this complex with two equivalents of 2,6-diethynylpyridine under CuAAC conditions. Disappointingly, despite trialling various catalysts, solvents and transition metal ion templates (Zn^{2+}, Co^{2+}, Ni^{2+}) we never observed any evidence of catenane formation. Computational modelling (molecular dynamics calculations at a semi-empirical level of theory using the GFN2-xTB methodology[47]) of the putative catenanes suggest that their structures are at least feasible, *i.e.* modelled structures do not reveal any obviously unlikely bond lengths or angles, or any significant steric clashes (see Section 4 of the ESI). Given this, we are not entirely sure why catenane formation was not observed. We note that Gunnlaugsson observed that hydrogen bonded self-templation of **btp** [2]catenanes was very dependent on both precursor geometry[39] and macrocycle ring size.[38] In some cases, even when favourable solution self-association was observed, no interlocked product was formed.[39] We see a similar phenomenon in our system, where clear formation of an ML_2 precursor species is observed, but no catenane forms.

Synthesis of tetratriazole macrocycle 3 and formation of solid state nanotube structure

Given the lack of success of catenane formation, we prepared and isolated the tetratriazole macrocycle **3**. This macrocycle has very low solubility in all tested solvents, which hampered its purification. Initially we sought to overcome these problems by maximizing the yield of macrocycle and thus minimizing the amount of purification required. To this end, we reacted mono-protected diethynylpyridine **4** (see ESI for synthesis) with **1** to synthesize compound **5** containing a TIPS-protected alkyne and azide group (Scheme 2). Subsequent deprotection using TBA·F gave **6** containing an alkyne and azide group. Intramolecular CuAAC cyclisation at low concentrations (0.5 mM) in a mixture of chloroform and methanol gave pure macrocycle in remarkably high yield (84%) after removal of the copper catalyst using EDTA/$NH_{3(aq)}$ and purification by column chromatography.

While this approach gives a very high yield of macrocycle in the cyclisation step, the synthesis of precursors **4** – **6** is tedious and time-consuming. We have subsequently found that the low solubility of the macrocycle makes purification facile, even if there is relatively little macrocycle present in a reaction mixture. Reacting **btp** diazide **1** with diethynylpyridine gives the macrocycle in approximately 20% yield after removal of the copper catalyst and recrystallisation from hot DMF (Scheme 3). While this approach is considerably lower yielding, it requires fewer synthetic steps and purification is considerably easier. Indeed, it is even possible to isolate small quantities of pure **3** by simply reacting diethynylpyridine and **1** and purifying by recrystallisation, although yields in this case are very low (3%, full details are provided in the ESI).

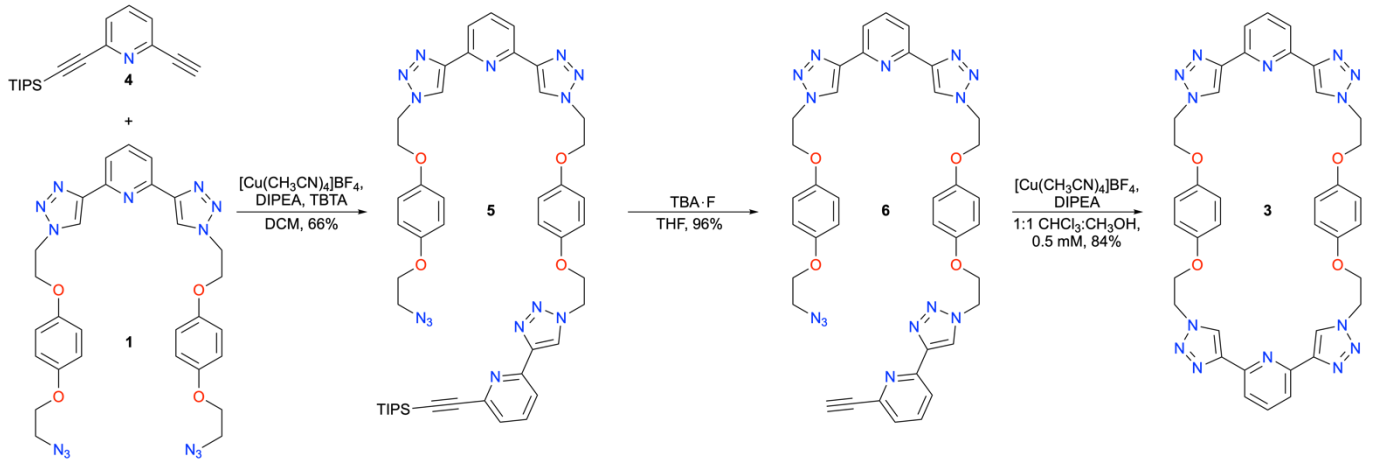

Scheme 2 Synthesis of tetratriazole macrocycle **3** in high yield using an intramolecular coupling strategy.

Unfortunately, the macrocycle has very low solubility in all tested solvents, which ruled out interrogation of its guest binding properties. It has some solubility in DMF (< 1 mg mL^{-1}) and DMSO (< 2 mg mL^{-1}), and we were able to grow single crystals by slowly cooling a hot DMF solution of the macrocycle. X-ray crystallography revealed that in the solid state the macrocycle has a boat-like structure and that these macrocycles stack to give the tube-like structure shown in Figure 4. Interestingly, even though the nanotubes have very low solubility (suggestive of strong intermolecular interactions), there are no particularly short inter-macrocycle hydrogen bonds in the solid state structure. Indeed, the only hydrogen bonding interactions shorter than the sum of the van der Waals radii are interactions between CH_2 groups next to triazole rings and triazole nitrogen atoms on an adjacent macrocycle (H-N = 2.39, 2.49 Å, 84 and 87% of the sum of the van der Waals radii of H and N[48]). Two solvent molecules are located inside each macrocycle's cavity and there is a relatively weak contact between the DMF oxygen atom and a triazole C–H hydrogen atom (H-O = 2.57 Å, 90% of the sum of the van der Waals radii of H and O[48]).

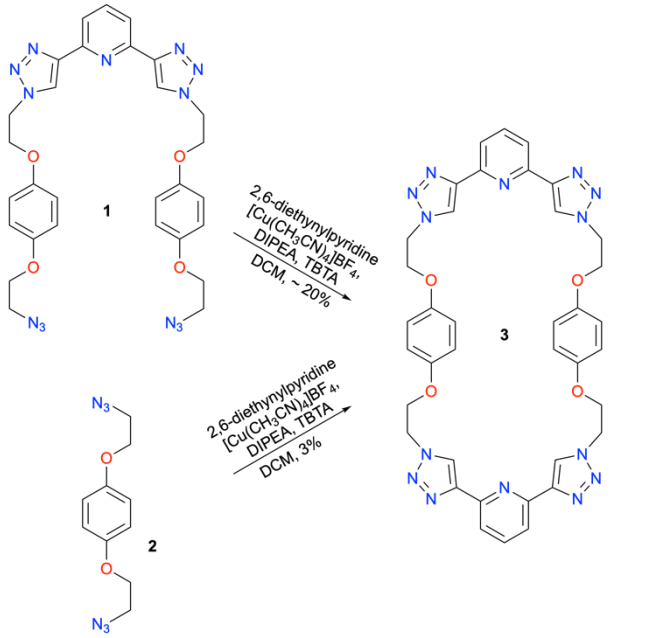

Scheme 3 Low yielding but facile syntheses of **3**.

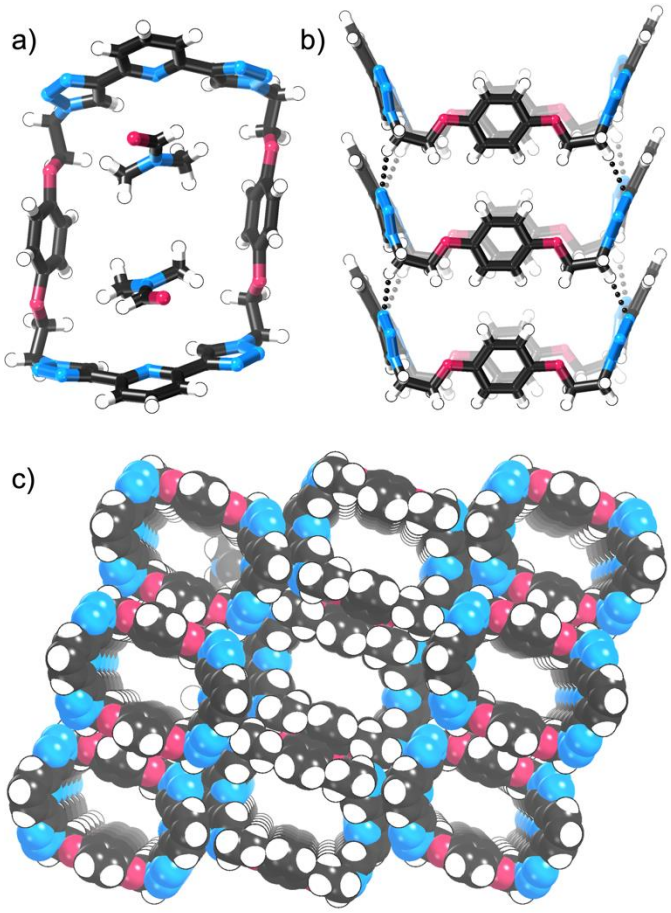

Figure 4 Views of the solid state structure of **3**: a) view of a single macrocycle and DMF solvates; b) view showing inter-macrocycle C–H-N hydrogen bonds; c) spacefilling view of nanotube structure.

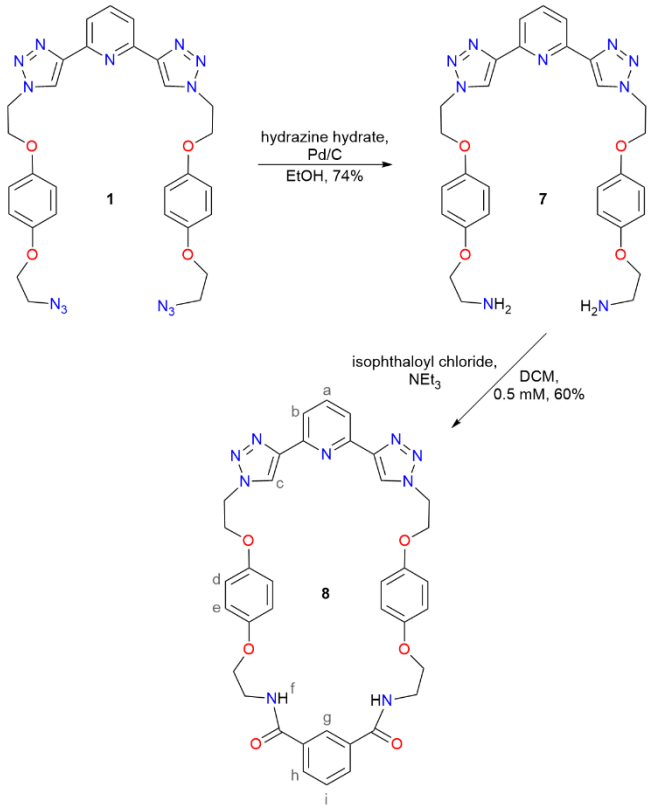

Scheme 4 Synthesis of **btp** diamide macrocycle **8**.

Synthesis of btp diamide macrocycle 8

Given the poor solubility of bis-**btp** macrocycle **3**, we next investigated the synthesis of a macrocycle containing only a single **btp** motif. We reduced the diazide **1** to the corresponding diamine **7** in 74% yield (Scheme 4), and then conducted an amide condensation reaction with isophthaloyl chloride in dilute (0.5 mM) dichloromethane solution containing triethylamine. After purification by preparative TLC, this gave the new macrocycle **8** in 60% yield. This macrocycle was characterized by ^{1}H and ^{13}C NMR spectroscopy, high resolution ESI mass spectrometry and X-ray crystallography.

Single crystals of **8** were obtained by vapour diffusion of diethyl ether into a solution of the macrocycle in a mixture of dichloromethane, DMSO and methanol. The resulting crystal structure contains both DMSO and dichloromethane solvents, with the oxygen atom of the DMSO hydrogen bonding to the isophthalamide N–H donors (H-O distances: 2.15, 2.21 Å, 80, 82% of the sum of the van der Waals radii of H and O[48]). Similarly to **3**, the solid state structure of **8** is boat-like (Figure 5a), although in this case, the boats do not stack into extended nanotubes.

Anion recognition properties of 8

Halide anion recognition: Macrocycle **8** contains **btp** and isophthalamide[49] motifs, both of which have been shown to bind anions. We investigated the ability of **8** to bind halide anions in the polar aprotic solvent CD_3CN using ^{1}H NMR spectroscopy. Potentially, the anion could be complexed at either the **btp** or isophthalamide sites, or a mixture of the two. Addition of tetrabutylammonium chloride (TBA·Cl) to **8** caused relatively large downfield shifts of the isophthalamide N–H and interior phenylene C–H proton resonances, consistent with hydrogen bonding with the anion (Figure 6). Interestingly while these shifts are substantial, no evidence of any interaction whatsoever is observed for the **btp** group. In this "intramolecular" competition experiment, it is clear that the amide donors of the isophthalamide motif dominate. Addition of bromide and iodide results in similar downfield shifts, although of a lesser magnitude. Fitting the movement of the amide and phenylene proton resonances to a 1:1 binding isotherm using *Bindfit*[50] gave the association constants

shown in Table 1 (full details including URLs for *Bindfit* fitting are provided in Section 2.4 of the ESI) . Unsurprisingly the smallest halide binds most strongly. Association constants are lower than those recorded in acetone for isophthalamide macrocycles that do not contain the **btp** motif (*e.g.* K_a ~ 2,500 M^{-1} for Cl^- in acetone),[51] which we attribute to the more polar solvent used in our studies. It does not appear that the **btp** has a significant effect on the anion recognition properties of the isophthalamide motif.

We obtained crystals of the bromide complex of **8** by vapour diffusion of diethyl ether into a CD_3CN titration sample containing **8** and a large excess of TBA·Br. The X-ray crystal structure of these crystals show that the Br^- anion binds at the isophthalamide part of the host, with no interactions observed with the **btp** motif. Hydrogen bonds between the amide donors and bromide anion are of moderate length (H-Br^- distances: 2.63 – 2.71 Å, 86 – 89% of the sum of the van der Waals radii[48]). Interestingly in this structure, the macrocycle does not fully take on a boat-like structure, with the isophthalamide end of the macrocycle instead lying approximately planar with the central portion of the macrocycle.

Recognition of dicarboxylates: We next investigated the binding of dicarboxylate anions.[52,53] These are important industrially and medically, and we reasoned that the benzene dicarboxylates, terephthalate (*i.e.* 1,4-benzenedicarboxylate) and isophthalate (*i.e.* 1,3-benzenedicarboxylate) may be able to bind to both the isophthalamide and **btp** motifs in **8**. Addition of either of these anions to **8** in CD_3CN resulted in very large downfield shifts of the isoophthalamide N–H and interior C–H resonances as well as those of the **btp** triazole motif, consistent with binding of the carboxylate groups to both of these recognition motifs (Figure 6). The macrocycle hydroquinone motif shifts significantly upfield, consistent with stacking interactions with the aromatic anions, implying that these anions are at least partially included within the cavity of the macrocycle. The association of these two dicarboxylates was too strong to measure by ^1H NMR titration experiments (K_a >> 10^4 M^{-1}). For comparison, we also studied the binding of the smaller dicarboxylate oxalate: this anion bound less strongly (K_a = 7670 ± 570 M^{-1}) and only at the isophthalamide part of the molecule with no binding at the **btp** group. The isophthalamide N–H resonance and interior phenylene resonance move downfield by 3.25 and 1.06 ppm during the course of the titration while the triazole C–H resonance shows negligible movement (0.01 ppm).

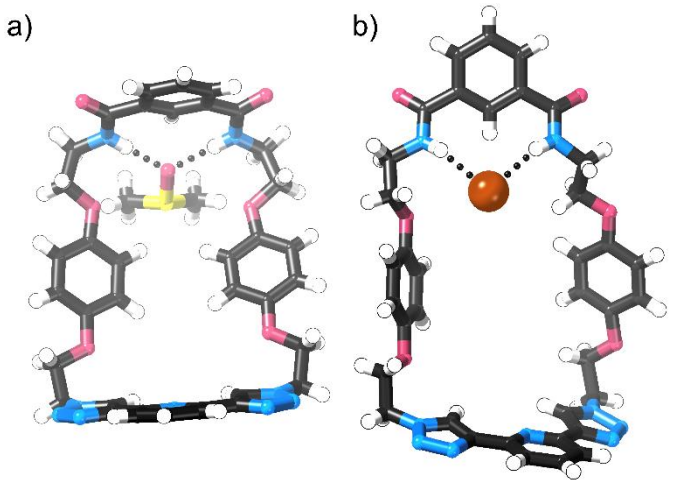

Figure 5 Views of the solid state structure of a) **8** and b) **8·Br⁻**. Dichloromethane solvate in the structure of **8** and all solvents and the TBA cations in the structure of **8·Br⁻** are omitted for clarity. Note, that the structure of **8·Br⁻** has Z′ = 2, only the lower-numbered macrocycle and anion are shown.

Encouraged by the very strong binding of terephthalate and isophthalate in the polar organic solvent CD_3CN, we next studied binding of terephthalate in 9:1 CD_3CN:D_2O. Unfortunately, no measurable binding was evident in this solvent mixture (isophthalamide C–H resonance shifts by 0.02 ppm and **btp** triazole resonance shifts by 0.01 ppm after ten equivalents of anion). Clearly even a relatively small percentage of water is sufficient to disrupt the hydrogen bonding interactions between the macrocycle and the anion.

Table 1. 1:1 Association constants for binding of halide anions to **8** in CD_3CN.[a]

Anion	K_a (M^{-1})	Binding site
Cl^-	396 ± 4	Isophthalamide only
Br^-	91 ± 2	Isophthalamide only
I^-	28 ± 1	Isophthalamide only
Terephthalate^{2-}	> 10^4	Isophthalamide and **btp**
Isophthalate^{2-}	> 10^4	Isophthalamide and **btp**
Oxalate^{2-}	7670 ± 570	Isophthalamide only

[a] Anions added as TBA^+ salts, binding constants determined using *Bindfit*,[50] ± values represent 95% confidence interval of K_a based on estimated asymptotic error.[54]

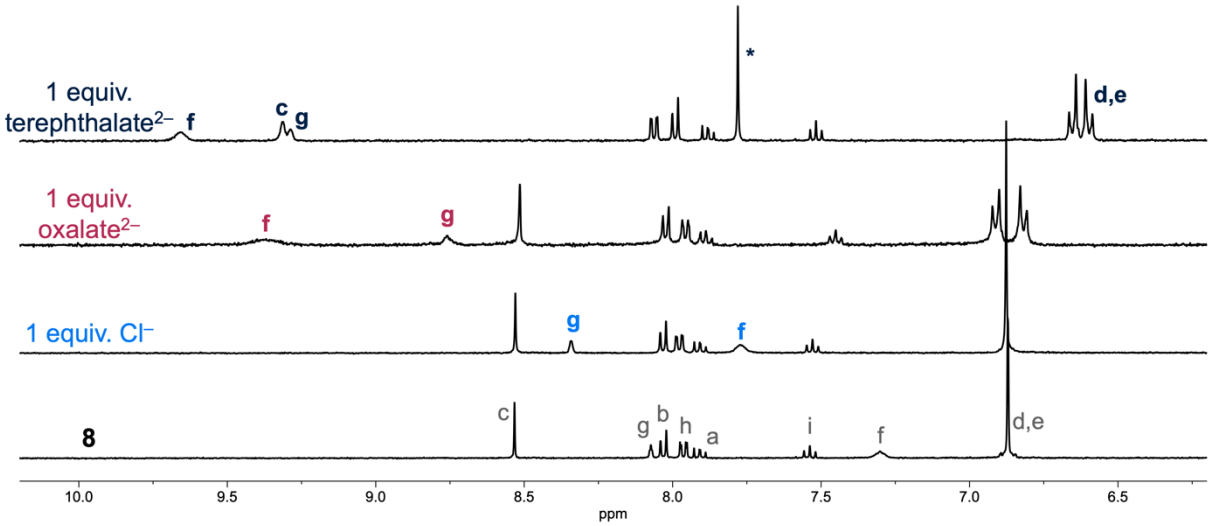

Figure 6 Partial ^{1}H NMR spectrum of **8** upon addition of TBA·Cl, TBA_2·oxalate or TBA_2·terephthalate (1.0 mM **8** in CD_3CN, 298 K, 400 MHz). Peaks that show significant movement on anion addition are labelled corresponding to atom labelling shown in Scheme 4; * indicates the peak arising from terephthalate anion.

Metal complexation by 8

As well as a potent isophthalamide hydrogen bonding motif, **8** contains the potentially terdentate **btp** ligand group. We thought that if we could complex metal cations to the **btp** motif, the resulting positive charge on the macrocycle metal complex may increase the relatively modest halide binding affinity of **8**. To this end, we first investigated the ability of **8** to complex the diamagnetic metal ions Zn(II) and Pd(II). ^{1}H NMR binding studies using $[Zn(OH_2)_6](ClO_4)_2$ revealed negligible binding in d_6-DMSO (Figure S26), while studies in 1:1 $CDCl_3$:CD_3OD showed significant peak shifts (Figure S25). The main complexation product is in fast exchange with **8** on the NMR timescale, but a minor by-product forms and is in slow exchange. Studies using $[Pd(CH_3CN)_4](BF_4)_2$ gave results that were easier to interpret with complexation in 1:1 $CDCl_3$:CD_3OD showing the sequential formation of two products that are in slow exchange with free **8** (Figure S27) and studies in d_6-DMSO showing the formation of a single species in slow exchange on the NMR timescale (Figure S28). Given the clean formation of a single complex using Pd(II) in d_6-DMSO, we attempted to isolate this; however precipitating a solid from DMSO resulted in a mixture of products. Instead we stirred **8** and $[Pd(CH_3CN)_4](BF_4)_2$ in acetonitrile, and precipitated using diethyl ether to give $[Pd{\cdot}\mathbf{8}{\cdot}CH_3CN](BF_4)_2$ in 66% yield. This was characterized by ^{1}H, ^{13}C and ^{19}F NMR spectroscopy, and high resolution ESI mass spectrometry, all of which were consistent with the expected product.

Anion complexation by $[Pd{\cdot}\mathbf{8}{\cdot}CH_3CN](BF_4)_2$

Solution phase studies: We studied the addition of the halide anions Cl^-, Br^- and I^- to $[Pd{\cdot}\mathbf{8}{\cdot}CH_3CN](BF_4)_2$ in CD_3CN. For all three halide anions, clean and quantitative conversion is seen to a new product that is in slow exchange with the starting complex on the ^{1}H NMR timescale. We assign these products as $[Pd{\cdot}\mathbf{8}{\cdot}X]BF_4$, where X is a halide anion that has replaced a coordinated acetonitrile solvent molecule, *i.e.* anion binding occurs initially at the metal ion. As shown in Figure 7, addition of one equivalent of chloride anion causes relatively small (~ 0.1 ppm) upfield shifts in the peaks corresponding to the triazole and pyridine C–H hydrogen atoms, which is consistent with the halide anion increasing electron density at the palladium centre and **btp** motif.

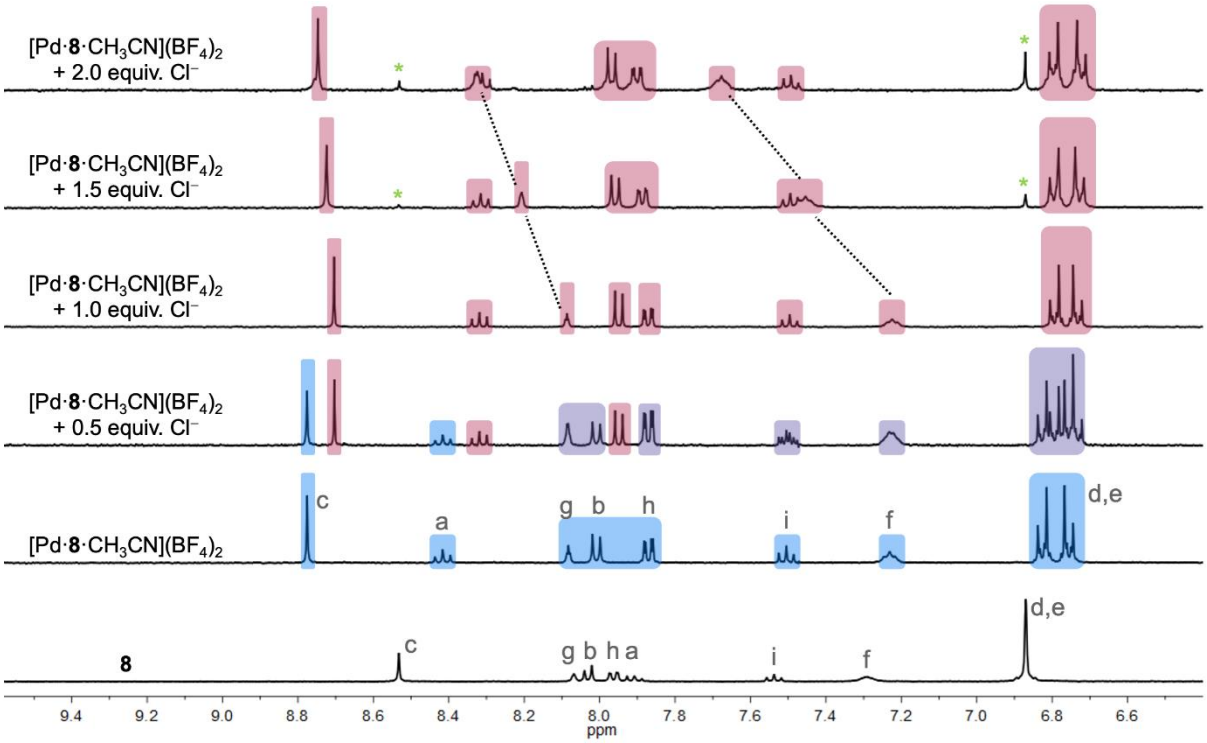

Figure 7 Partial ^{1}H NMR spectra of **8**, and [Pd·**8**·CH$_3$CN]BF$_4$ upon addition of TBA·Cl. Peak labelling corresponds to atom labelling shown in Scheme 4. Peaks corresponding to [Pd·**8**·CH$_3$CN](BF$_4$)$_2$ are coloured blue, peaks corresponding to [Pd·**8**·Cl]BF$_4$ are coloured maroon, and peaks corresponding to both are coloured purples. Peaks corresponding to the re-formation of uncomplexed **8** are indicated with green asterisks. An expanded version of this Figure including additional equivalents of Cl$^-$ and a wider spectral window is provided as Figure S41 (1.0 mM in CD$_3$CN, 298 K, 400 MHz).

Importantly, no change is observed in the isophthalamide C–H or N–H resonances, which is clear evidence that this part of the molecule does not participate in initial anion binding. Addition of further equivalents of chloride results in downfield shifts of the amide N–H resonance and the interior C–H resonance of the isophthalamide motif, consistent with binding of a second anion at this position (and similar to studies of the interaction of **8** and anions in the absence of the metal ion). Very similar trends are observed on addition of Br$^-$ or I$^-$ (Figure S42 and S43). In all cases, peaks corresponding to free macrocycle **8** appear upon addition of excess halide, which we attribute to precipitation of insoluble PdX$_2$ salts (small amounts of precipitation are visible in these samples). This is most notable with the largest halide, I$^-$. Clearly, complexation of Pd(II) does improve the binding properties of the macrocycle, although the utility of this is somewhat limited by precipitation of PdX$_2$ compounds.

Solid state crystal structures: We were able to obtain single crystals of [Pd·**8**·X]BF$_4$ (X = Cl$^-$, Br$^-$ and I$^-$) and characterized the solid state structures of these complexes using X-ray crystallography. We first obtained crystals for [Pd·**8**·Br]BF$_4$ by dissolving what was believed to be [Pd·**8**·DMSO](BF$_4$)$_2$ in either acetonitrile or 1:1 chloroform:methanol and subjecting these solutions to diethyl ether vapour diffusion (the two structures are essentially identical). It is unclear where the adventitious Br$^-$ anion comes from, although we suspect it may be due to impurities in the commercial sample of [Pd(CH$_3$CN)$_4$](BF$_4$)$_2$ used. Attempts to isolate pure [Pd·**8**·solvent](BF$_4$)$_2$ using older bottles of the palladium(II) reagent were plagued by irreproducibility, and it was necessary to use a fresh bottle to achieve reproducible synthesis of clean [Pd·**8**·CH$_3$CN](BF$_4$)$_2$. Once this was accomplished, [Pd·**8**·Cl]BF$_4$ and [Pd·**8**·I]BF$_4$ were readily crystallised by vapour diffusion of diethyl ether into an acetonitrile solution containing a 1:1 mixture of [Pd·**8**·CH$_3$CN](BF$_4$)$_2$ and TBA·Cl or TBA·I.

The structure of [Pd·**8**·Cl]BF_4 features the expected square planar palladium(II) centre with the **btp** motif of **8** providing a terdentate pocket and the chloride anion completing the coordination sphere (Figure 8a). The macrocycle retains the boat-like structure seen in the crystal structure of the free macrocycle, and there is a close Pd–Pd contact in the solid state (3.39 Å, 79% of the sum of the van der Waals radii of two Pd atoms[48]), which links the complexes into dimers. The isophthalamide amide groups do not form any significant hydrogen bonds. The structure of [Pd·**8**·I]BF_4 is very similar to that of [Pd·**8**·Cl]BF_4, except that no significant Pd–Pd contact is observed.

The structure of [Pd·**8**·Br]BF_4 is quite different from the Cl^- and I^- complexes, and consists of dimers of macrocycles, which are assembled through N–H–Br^- hydrogen bonding between the isophthalamide motifs and coordinated Br^- anions (Figure 8b). These dimers are then further linked into 1D "chains of dimers" through short Pd–Pd contacts (3.29 Å, 77% of the sum of the van der Waals radii of two Pd atoms[48]). This dimeric assembly is unusual, but appears to be a solid state phenomenon, as the ^{1}H NMR spectrum of [Pd·**8**·Br]BF_4 shows no evidence of amide hydrogen bonding in CD_3CN solution. It is unclear what promotes the formation of this complex assembly in the solid state, but it is notable that it forms upon crystallisation from either CH_3CN or 1:1 $CHCl_3$:CH_3OH.

The structures of [Pd·**8**·Cl]BF_4 and [Pd·**8**·Br]BF_4 both feature quite short Pd–Pd contacts in the solid state. We note that these metallophilic interactions are likely to be vanishingly small in solution.[55] Two previous Pd **btp** complexes have been characterized by X-ray crystallography, and neither of these feature close Pd–Pd contacts,[30,56] although we note that generally these contacts are relatively common for palladium(II) complexes with nitrogen containing ligands. The contact distances observed in our systems are at the shorter end of the range of those in the Cambridge Structural Database[57] (see ESI).

Conclusions

The **btp** diazide **1** was prepared and shown to form ML_2 complexes with Zn^{2+}, however attempts to use transition metal templation to form a catenane from this assembly were unsuccessful. Instead, it was possible to isolate this bis-**btp** macrocycle **3** in very high yields (84%) under dilute conditions using a stepwise procedure. Alternate strategies gave **3** in much lower yields but required much shorter synthetic pathways; X-ray crystallography revealed that **3** has a solid state nanotube structure. Reduction of **1** gave the **btp** diamine **7**, which was used to prepare **btp**-isophthalamide macrocycle **8**. This macrocycle binds halide anions with modest strength and dicarboxylate anions strongly in the polar organic solvent CD_3CN. When coordinated to Pd^{2+} the resulting complex binds strongly to halide anions, but at the vacant coordination site of the metal ion rather than the isophthalamide motif. These palladium(II) halide complexes formed interesting solid state structures, several of which contained short Pd–Pd contacts. This investigation demonstrates the versatility of the **btp** motif in supramolecular chemistry.

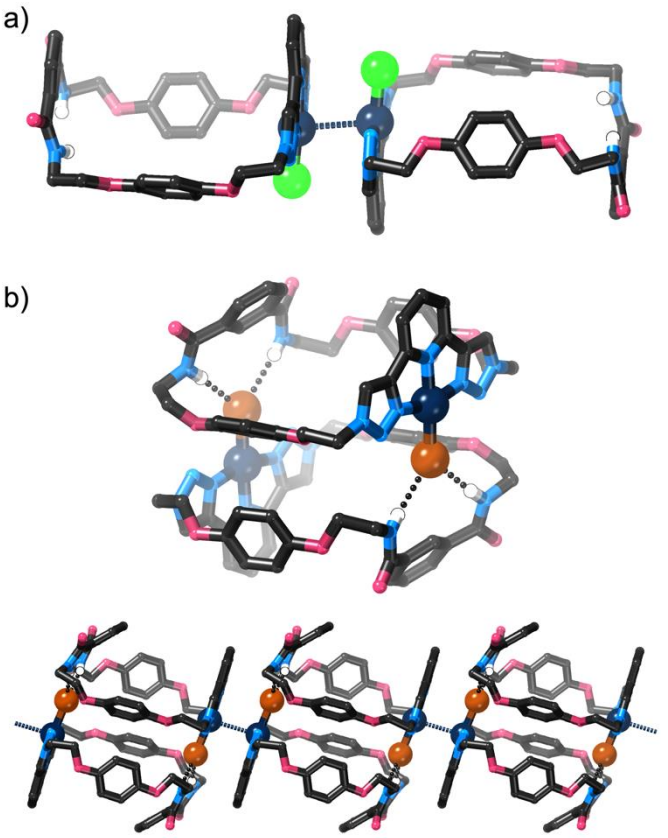

Figure 8 X-ray crystal structures of a) [Pd·**8**·Cl]BF_4 and b) [Pd·**8**·Br]BF_4. Solvent molecules and most hydrogen atoms omitted for clarity. The structure of [Pd·**8**·I]BF_4 is very similar to that of [Pd·**8**·Cl]BF_4 but does not feature a short Pd–Pd contact (Figure S50).

Experimental section

General remarks

TBTA[58] and 2,6-diethynyl pyridine[59] were prepared as previously described. Diazide **2**[60] and TIPS-protected 2,6-diethynylpyridine **4**[61] are known compounds but were prepared by new methods; details of these syntheses are provided in the ESI. **Azides and perchlorates are potentially explosive; no issues were encountered during this work but the use of care and small reaction scales is recommended.** Details of instrumentation, ^{1}H and ^{13}C NMR spectra for new compounds, details of anion binding and metal complexation studies, computational calculations and X-ray crystallography are provided in the ESI. Crystallographic data have been deposited with the Cambridge Crystallographic Data Centre (CCDC numbers: 2225115 – 2225221 and 2225744).

Diazide 1: To a deoxygenated solution of **2** (2.33 g, 9.4 mmol) in CH_2Cl_2 (20 mL) were added 2,6-diethynylpyridine (0.127 g, 1.00 mmol), $[Cu(MeCN)_4](BF_4)$ (0.015 g, 0.050 mmol) and DIPEA (0.16 mL, 0.12 g, 0.94 mmol). The solution was stirred for 4 days at room temperature and then a solution of EDTA/$NH_{3(aq)}$ (0.05 M EDTA, 1.0 M NH_3, 10 mL) was added. After 10 min of stirring, the layers were separated and the

organic phase was dried over anhydrous $MgSO_4$. The solvent was removed under vacuum and the crude material was purified by careful column chromatography (eluent: 199:1 CH_2Cl_2:CH_3OH) to give **1** (0.527 g, 84%) as a white solid.

^{1}H NMR (400 MHz, $CDCl_3$): 8.34 (s, 2H), 8.08 (d, *J* = 7.8 Hz, 2H), 7.84 (t, *J* = 7.8 Hz, 1H), 6.81 (s, 8H), 4.79 (t, *J* = 5.1 Hz, 4H), 4.36 (t, *J* = 5.1 Hz, 4H), 4.05 (t, *J* = 5.0 Hz, 4H), 3.53 (t, *J* = 5.0 Hz, 4H) ppm. ^{13}C NMR (101 MHz, $CDCl_3$): *δ*= 153.2, 152.6, 150.1, 148.5, 137.8, 123.4, 119.5, 116.0, 115.8, 67.7, 67.3, 50.3, 50.1 ppm. HRESI-MS (pos.): 624.2557, calc. for $[C_{29}H_{29}N_{13}O_4{\cdot}H]^+$ = 624.2544 Da.

TIPS-protected azide alkyne 5: To a degassed solution of **4** (53 mg, 0.19 mmol) in CH_2Cl_2 (20 mL) were added **1** (645 mg, 1.03 mmol), $[Cu(MeCN)_4](PF_6)$ (11 mg, 0.036 mmol), TBTA (19 mg, 0.036 mmol) and DIPEA (31 µL, 23 mg, 0.18 mmol). The solution was stirred for 17 h at room temperature and then a solution of EDTA/$NH_{3(aq)}$ (0.05 M EDTA, 1 M NH_3, 20 mL) was added. The resulting mixture was stirred for 10 min and the layers were separated. The organic layer was dried over anhydrous $MgSO_4$ and the solvent was removed under reduced pressure. The crude material was purified by column chromatography (eluent: 99:1 CH_2Cl_2:CH_3OH) to give **5** (112 mg, 66%) as a white solid.

^{1}H NMR (400 MHz, $CDCl_3$): 8.33 (m, 3H), 8.05 (m, 3H), 7.79 (t, *J* = 7.8 Hz, 1H), 7.66 (t, *J* = 7.8 Hz, 1H), 7.37 (d, J = 7.7 Hz, 1H), 6.73 (m, 8H), 4.75 – 4.65 (m, 6H), 4.32 – 4.22 (m, 6H), 4.00 (t, *J* = 5.0 Hz, 2H), 3.48 (t, *J* = 5.0 Hz, 2H), 1.12 (m, 21H) ppm . ^{13}C NMR (101 MHz, $CDCl_3$):153.1, 152.7, 152.6, 152.5, 150.5, 150.0, 148.4, 147.9, 143.0, 137.7, 136.8, 127.0, 123.8, 123.31, 123.30, 119.5, 119.2, 115.85, 115.81, 115.77, 115.70, 106.1, 91.7, 67.6, 67.2, 67.1, 66.9, 50.2, 50.0, 49.94, 49.90, 18.7, 11.3 ppm (some aryl environments overlapping/not detected). ESI-MS (pos.): 929.9, calc. for $[C_{47}H_{54}N_{14}O_4Si{\cdot}Na]^+$ = 929.4 Da.

Azide alkyne 6: To a deoxygenated solution of **5** (87 mg, 0.096 mmol) in THF (20 mL) was added a solution of TBA·F in THF (1.0 M, 0.29 mL, 0.29 mmol). The solution was stirred at room temperature for 16 hours under a nitrogen atmosphere and subsequently concentrated to dryness under reduced pressure. The crude material was purified by column chromatography (eluent: 96:4 CH_2Cl_2:CH_3OH) to yield **6** as a white solid. Yield: 69 mg (0.092 mmol, 96%).

^{1}H NMR (400 MHz, $CDCl_3$): 8.37 (s, 1H), 8.33 (d, *J* = 4.7 Hz), 8.16 (d, *J* = 7.8 Hz, 1H), 8.07 (d, *J* = 7.8 Hz, 2H), 7.84 (t, *J* = 7.8 Hz, 1H), 7.73 (t, *J* = 7.8 Hz, 1H), 7.41 (d, *J* = 7.8 Hz, 1H), 6.76 – 6.83 (m, 8H), 4.73 – 4.81 (m, 6H), 4.34 – 4.38 (m, 4H), 4.31 (t, *J* = 5.1 Hz, 2H), 4.05 (t, *J* = 5.0 Hz, 2H), 3.53 (t, *J* = 5.0 Hz, 2H), 3.17 (s, 1H) ppm. ^{13}C NMR (101 MHz, $CDCl_3$): 153.3, 152.9, 152.8, 152.6, 150.9, 150.0, 148.4, 147.9, 142.0, 138.0, 137.2, 126.8, 123.8, 123.5, 120.2, 119.6, 119.50, 116.06, 116.00, 115.9, 67.8, 67.4, 67.3, 67.0, 50.3, 50.19, 50.16, 50.1 ppm (some aryl environments overlapping/not detected). HRESI-MS (pos.): 751.2981, calc. for $[C_{38}H_{34}N_{14}O_4{\cdot}H]^+$ = 751.2966 Da.

Tetra-triazole macrocycle 3: To a deoxygenated solution of **6** (101 mg, 0.13 mmol) in $CHCl_3$/MeOH (1:1, 250 mL) was added $[Cu(CH_3CN)_4]BF_4$ (9 mg, 0.03 mmol) and DIPEA (26 µL, 19 mg, 0.15 mmol). The mixture was stirred for 16 hours at room temperature under a nitrogen atmosphere. Subsequently, EDTA/$NH_{3(aq)}$ (0.05 M EDTA, 1.0 M NH_3, 50 mL) was added and the resulting mixture was stirred for 10 min. The mixture was diluted with H_2O (200 mL) and the layers were separated. The organic layer was dried over anhydrous $MgSO_4$ and the solvent was removed under vacuum. The crude material was purified by column chromatography (96:4 CH_2Cl_2:CH_3OH) to afford **3** as a white solid. Yield: 85 mg (0.11 mmol, 84%).

^{1}H NMR (400 MHz, DMSO-*d*$_6$): 8.73 (s, 4H), 7.96–7.99 (m, 6H), 6.86 (s, 8H), 4.85 (t, *J* = 5.0 Hz, 8H), 4.35 (t, *J* = 5.0 Hz, 8H) ppm. HRESI-MS (pos.): 751.2957, calc. for. $[C_{38}H_{34}N_{14}O_4{\cdot}H]^+$ = 751.2966 Da.

Unfortunately, the compound was too insoluble to acquire ^{13}C NMR data (we have found that DMSO is the best solvent for this compound, but even then the solubility is < 2 mg mL^{-1}).

*Lower yielding procedures for the synthesis of this compound directly from **1** and 2,6-diethynylpyridine or **2** and 2,6-diethynylpyridine are provided in the Supporting Information.*

Diamine 7: The diazide **1** (125 mg, 0.200 mmol) was dissolved in ethanol (20 mL) and Pd/C (5%, 13 mg) was added followed by hydrazine hydrate (0.5 mL, excess). The resulting dark suspension was heated to reflux under a nitrogen atmosphere for 3 hours, then cooled to room temperature and filtered through a short pad of celite. The celite was washed with ethanol (10 mL) and ethyl acetate (2 × 10 mL) and the combined filtrates were taken to dryness to give a waxy white solid. Ethyl acetate (5 mL) was added to this solid and the resulting white suspension sonicated for 30 minutes. It was filtered to give a white powder, which was washed with ethyl acetate (2 × 2 mL) and thoroughly air-dried to give **7**. Yield: 85 mg (0.15 mmol, 74%).

^{1}H NMR (400 MHz, DMSO-*d*$_6$): 8.71 (s, 2H), 7.95–8.01 (m, 3H), 6.82–6.88 (m, 8H), 4.84 (t, *J* = 5.1 Hz, 4H), 4.42 (t, *J* = 5.1 Hz, 4H), 3.82 (t, *J* = 5.8 Hz, 4H), 2.81 (t, *J* = 5.8 Hz, 4H) ppm. ^{13}C NMR (101 MHz, DMSO-*d*$_6$): 153.1, 151.9, 149.9, 147.1, 138.3, 123.9, 118.4, 115.7, 115.4, 70.4, 66.7, 52.0, 49.5 ppm. HRESI-MS (pos.): 594.2563, calc. for $[C_{29}H_{33}N_9O_4{\cdot}Na]^+$ = 594.2553 Da.

Ditriazole diamide macrocycle 8: Btp diamine **7** (57 mg, 0.10 mmol) was suspended in dichloromethane (180 mL); triethylamine (69 µL, 51 mg, 0.50 mmol) was added and the suspension sonicated to ensure dispersion of the diamine. A solution of isophthaloyl chloride (20 mg, 0.10 mmol) in dichloromethane (20 mL) was added in one portion and the resulting pale suspension stirred at room temperature under a nitrogen atmosphere for 3 days. After this time, the solvent was removed under reduced pressure, and the resulting pale waxy solid purified by preparative TLC (eluent: 96:4 CH_2Cl_2:CH_3OH) to give **8** as a white powder. Yield: 42 mg (0.060 mmol, 60%).

^{1}H NMR (d_6-DMSO): 8.69–8.74 (m, 4H), 8.29 (br. s, 1H), 7.96–8.00 (m, 3H), 7.94 (dd, *J* = 7.7, 1.5 Hz, 2H), 6.87 (s, 8H), 4.85 (t, *J* = 5.1 Hz, 4H), 4.37 (t, *J* = 5.1 Hz, 4H), 4,04 (t, *J* = 5.3 Hz, 4H), 3.61 (app. q, *J* = 5.3 Hz, 4H). ^{13}C NMR (d_6-DMSO): 168.2, 153.0, 152.1, 149.9, 147.2, 138.3, 134.5, 130.0, 128.5, 125.9, 123.8, 118.4, 115.6, 115.5, 66.9, 66.6, 49.6 ppm (*one alkyl resonance overlapping/not observed*). HRESI-MS (pos.): 702.2767, calc. for $[C_{37}H_{35}N_{19}O_6{\cdot}H^+]$ = 702.2789 Da.

Palladium(II) complex of 8, [Pd·8·MeCN](BF$_4$)$_2$: Acetonitrile (1 mL) was added to macrocycle **8** (7.0 mg, 0.010 mmol) and [Pd(MeCN)$_4$](BF$_4$)$_2$ (4.9 mg, 0.011 mmol) in a screwtop vial. This initially resulted in the formation of a pale suspension, but after approximately one minute all material dissolved to give a clear yellow solution. The reaction was stirred for 30 minutes, and then the solution was added to diethyl ether (3 mL) resulting in the formation of a yellow precipitate. This was left to stand for 30 minutes, then isolated by filtration, washed with diethyl ether (2 × 1 mL) and dried *in vacuo* to give [Pd·**8**·MeCN](BF$_4$)$_2$ as a pale yellow powder. Yield: 6.7 mg (0.0066 mmol, 66%).

^{1}H NMR (CD_3CN): 8.78 (s, 2H), 8.42 (t, *J* = 8.1 Hz, 1H), 8.08 (t, *J* = 1.7 Hz, 1H), 8.01 (d, *J* = 8.1 Hz, 2H), 7.87 (dd, *J* = 7.8, 1.7 Hz, 2H), 7.50 (t, *J* = 7.7 Hz, 1H), 7.23 (t, *J* = 5.6 Hz, 2H), 6.74 – 6.84 (m, 8H), 4.94 (t, *J* = 4.7 Hz, 4H), 4.39 (t, *J* = 4.7 Hz, 4H), 4.05 (t, *J* = 4.5 Hz, 4H), 3.64 (app. q, *J* = 5.6 Hz, 4H) ppm. ^{13}C NMR (CD_3CN): 167.3, 154.6, 153.2, 150.0, 149.2, 146.4, 135.8, 130.6, 129.7, 129.2, 126.8, 123.1, 67.9, 67.7, 54.3, 40.0 ppm. ^{19}F NMR (CD_3CN): –151.6 – –151.7 (m) ppm. HRESI-MS (pos.): 403.5873, calc. for $[C_{37}H_{35}N_9O_6Pd]^{2+}$ = 403.5879; 842.1450, calc. for $[C_{37}H_{35}N_9O_6Pd{\cdot}Cl]^+$ = 842.1444; 852.1726, calc. for $[C_{37}H_{35}N_9O_6Pd{\cdot}CHO_2]^+$ = 852.1735 Da.

Conflicts of interest

There are no conflicts to declare.

Acknowledgements

We thank Dr Daniel Preston (ANU) for assistance with preparing POVRay images and useful discussions regarding Pd(II) coordination chemistry and Gareth Nelmes (ANU) and Dr Jamie Hicks (ANU) for assistance with synchrotron X-ray crystallography. A. H. G. D. acknowledges the Conseil régional de Bretagne ("Jeunes à l'international" grant). Parts of this work were conducted on the MX1[62] and MX2[63] beamlines of the Australian Synchrotron and made use of the Australian Cancer Research Foundation detector. Parts of this research were undertaken using the National Computational Infrastructure (NCI), which is supported by the Australian Government.

Notes and references

1 Z. Liu, S. K. M. Nalluri and J. F. Stoddart, *Chem. Soc. Rev.*, 2017, **46**, 2459–2478.
2 J. F. Stoddart, *Chem. Soc. Rev.*, 2009, **38**, 1802.
3 J. F. Stoddart, *Angew. Chem. Int. Ed.*, 2017, **56**, 11094–11125.
4 J.-P. Sauvage, *Angew. Chem. Int. Ed.*, 2017, **56**, 11080–11093.
5 K. N. Rose, *Chem. Commun.*, 1998, 407–408.
6 K. Murayama, *Chem. Commun.*, 1998, 607–608.
7 D. T. Bong and M. R. Ghadiri, *Angew. Chem. Int. Ed*, 2001, **40**, 2163–2166.
8 K. Nakamura, H. Okubo and M. Yamaguchi, *Org. Lett.*, 2001, **3**, 1097–1099.
9 S. Klyatskaya, N. Dingenouts, C. Rosenauer, B. Müller and S. Höger, *J. Am. Chem. Soc.*, 2006, **128**, 3150–3151.
10 J. N. Smith, C. Ennis and N. T. Lucas, *Chem. Sci.*, 2021, **12**, 11858–11863.
11 E. Saridakis, E.-M. Kasimati, K. Yannakopoulou and I. M. Mavridis, *Chem. Commun.*, 2022, **58**, 5300–5303.
12 L. R. MacGillivray and J. L. Atwood, *Nature*, 1997, **389**, 469–472.
13 M. R. Ghadiri, J. R. Granja, R. A. Milligan, D. E. McRee and N. Khazanovich, *Nature*, 1993, **366**, 324–327.
14 L. S. Shimizu, M. D. Smith, A. D. Hughes and K. D. Shimizu, *Chem. Commun.*, 2001, 1592–1593.
15 P. D. Frischmann, S. Guieu, R. Tabeshi and M. J. MacLachlan, *J. Am. Chem. Soc.*, 2010, **132**, 7668–7675.
16 Y. Yang, W. Feng, J. Hu, S. Zou, R. Gao, K. Yamato, M. Kline, Z. Cai, Y. Gao, Y. Wang, Y. Li, Y. Yang, L. Yuan, X. C. Zeng and B. Gong, *J. Am. Chem. Soc.*, 2011, **133**, 18590–18593.
17 Z. Liu, M. Frasconi, J. Lei, Z. J. Brown, Z. Zhu, D. Cao, J. Iehl, G. Liu, A. C. Fahrenbach, Y. Y. Botros, O. K. Farha, J. T. Hupp, C. A. Mirkin and J. Fraser Stoddart, *Nat. Commun.*, 2013, **4**, 1855.
18 X. Wu, P. Wang, P. Turner, W. Lewis, O. Catal, D. S. Thomas and P. A. Gale, *Chem*, 2019, **5**, 1210–1222.
19 J. P. Byrne, J. A. Kitchen and T. Gunnlaugsson, *Chem. Soc. Rev.*, 2014, **43**, 5302–5325.
20 A. F. Henwood, I. N. Hegarty, E. P. McCarney, J. I. Lovitt, S. Donohoe and T. Gunnlaugsson, *Coord. Chem. Rev.*, 2021, **449**, 214206.
21 N. G. White and P. D. Beer, *Chem. Commun.*, 2012, **48**, 8499.
22 M. J. Langton, S. W. Robinson, I. Marques, V. Felix and P. D. Beer, *Nat. Chem.*, 2014, **6**, 1039–1043.
23 S. W. Robinson, C. L. Mustoe, N. G. White, A. Brown, A. L. Thompson, P. Kennepohl and P. D. Beer, *J. Am. Chem. Soc.*, 2015, **137**, 499–507.
24 Y. Li, J. C. Huffman and A. H. Flood, *Chem. Commun.*, 2007, 2692.
25 R. M. Meudtner, M. Ostermeier, R. Goddard, C. Limberg and S. Hecht, *Chem. Eur. J.*, 2007, **13**, 9834–9840.
26 . Yuan, X. Fang, L. Zhang, G. Hong, Y. Lin, Q. Zheng, Y. Xu, Y. Ruan, W. Weng, H. Xia and G. Chen, *J. Mater. Chem.*, 2012, **22**, 11515–11522.
27 E. P. McCarney, J. P. Byrne, B. Twamley, M. Martínez-Calvo, G. Ryan, M. E. Möbius and T. Gunnlaugsson, *Chem. Commun.*, 2015, **51**, 14123–14126.
28 Y. Li, L. Chen, Y. Ai, E. Y.-H. Hong, A. K.-W. Chan and V. W.-W. Yam, *J. Am. Chem. Soc.*, 2017, **139**, 13858–13866.
29 D. A. W. Ross, D. Preston and J. D. Crowley, *Molecules*, 2017, **22**, 1762.
30 D. Preston and P. E. Kruger, *Chem. Eur. J.*, 2019, **25**, 1781–1786.
31 S.-Y. Wu, X.-Q. Guo, L.-P. Zhou and Q.-F. Sun, *Inorg. Chem.*, 2019, **58**, 7091–7098.
32 P. Weßling, M. Trumm, E. Macerata, A. Ossola, E. Mossini, M. C. Gullo, A. Arduini, A. Casnati, M. Mariani, C. Adam, A. Geist and P. J. Panak, *Inorg. Chem.*, 2019, **58**, 14642–14651.
33 X. Xu, J. F. R. Van Guyse, V. V. Jerca and R. Hoogenboom, *Macromol. Rapid Commun.*, 2020, **41**, 1900305.

34 Y. Li, M. Pink, J. A. Karty and A. H. Flood, *J. Am. Chem. Soc.*, 2008, **130**, 17293–17295.
35 Q. Duan, W. Xia, C. Lin, Y. Pan and L. Wang, *Tetrahedron Lett.*, 2015, **56**, 4002–4006.
36 Y. Liu, F. C. Parks, W. Zhao and A. H. Flood, *J. Am. Chem. Soc.*, 2018, **140**, 15477–15486.
37 A. Bosmani, S. A. Pujari, C. Besnard, L. Guénée, A. I. Poblador-Bahamonde and J. Lacour, *Chem. Eur. J.*, 2017, **23**, 8678–8684.
38 J. P. Byrne, S. Blasco, A. B. Aletti, G. Hessman and T. Gunnlaugsson, *Angew. Chem. Int. Ed.*, 2016, **55**, 8938–8943.
39 E. P. McCarney, W. J. McCarthy, J. I. Lovitt and T. Gunnlaugsson, *Org. Biomol. Chem.*, 2021, **19**, 10189–10200.
40 E. P. McCarney, J. I. Lovitt and T. Gunnlaugsson, *Chem. Eur. J.* 2021, **27**, 12052–12057.
41 A. J. McConnell and P. D. Beer, *Angew. Chem. Int. Ed.*, 2012, **51**, 5052–5061.
42 A. J. McConnell, A. Docker and P. D. Beer, *ChemPlusChem*, 2020, **85**, 1824–1841.
43 D. B. Amabilino, P. R. Ashton, V. Balzani, S. E. Boyd, A. Credi, J. Y. Lee, S. Menzer, J. F. Stoddart, M. Venturi and D. J. Williams, *J. Am. Chem. Soc.*, 1998, **120**, 4295–4307.
44 J. A. Berrocal, L. M. Pitet, M. M. L. Nieuwenhuizen, L. Mandolini, E. W. Meijer and S. Di Stefano, *Macromolecules*, 2015, **48**, 1358–1363.
45 Q. Wu, P. M. Rauscher, X. Lang, R. J. Wojtecki, J. J. de Pablo, M. J. A. Hore and S. J. Rowan, *Science*, 2017, **358**, 1434–1439.
46 N. D. Colley, M. A. Nosiglia, S. L. Tran, G. H. Harlan, C. Chang, R. Li, A. O. Delawder, Y. Zhang and J. C. Barnes, *ACS Cent. Sci.*, 2022, DOI: 10.1021/acscentsci.2c00697.
47 C. Bannwarth, S. Ehlert and S. Grimme, *J. Chem. Theory Comput.*, 2019, **15**, 1652–1671.
48 S. Alvarez, *Dalton Trans.*, 2013, **42**, 8617–8636.
49 K. Kavallieratos, S. R. de Gala, D. J. Austin and R. H. Crabtree, *J. Am. Chem. Soc.*, 1997, **119**, 2325–2326.
50 *Bindfit*, accessed at supramolecular.org.
51 M. R. Sambrook, P. D. Beer, J. A. Wisner, R. L. Paul, A. R. Cowley, F. Szemes and M. G. B. Drew, *J. Am. Chem. Soc.*, 2005, **127**, 2292–2302.
52 D. Curiel, M. Más-Montoya and G. Sánchez, *Coord. Chem. Rev.*, 2015, **284**, 19–66.
53 S. M. Butler and K. A. Jolliffe, *Org. Biomol. Chem.*, 2020, **18**, 8236–8254.
54 P. Thordarson, *Chem. Soc. Rev.*, 2011, **40**, 1305–1323.
55 Q. Zheng, S. Borsley, G. S. Nichol, F. Duarte and S. L. Cockroft, *Angew. Chem. Int. Ed.*, 2019, **58**, 12617–12623.
56 C. Lang, K. Pahnke, C. Kiefer, A. S. Goldmann, P. W. Roesky and C. Barner-Kowollik, *Polym. Chem.*, 2013, **4**, 5456.
57 R. Taylor and P. A. Wood, *Chem. Rev.*, 2019, **119**, 9427–9477.
58 T. R. Chan, R. Hilgraf, K. B. Sharpless and V. V. Fokin, *Org. Lett.*, 2004, **6**, 2853–2855.
59 A. Orita, K. Miyamoto, M. Nakashima, F. Ye and J. Otera, *Adv. Synth. Catal.*, 2004, **346**, 767–776.
60 D. E. Phipps and P. D. Beer, *Tetrahedron Lett.*, 2009, **50**, 3454–3457.
61 B. T. Holmes, P. Deb, W. T. Pennington and T. W. Hanks, *J. Polym. Res.*, 2006, **13**, 133–144.
62 N. P. Cowieson, D. Aragao, M. Clift, D. J. Ericsson, C. H. Gee, N. Mudie, S. Panjikar, J. R. Price, A. Riboldi-Tunnicliffe, R. Williamson and T. Caradoc-Davies, *J. Synchrotron Radiat.*, 2015, **22**, 187–190.
63 D. Aragao, J. Aishima, H. Cherukuvada, R. Clarken, M. Clift, N. P. Cowieson, D. J. Ericsson, C. L. Gee, S. Macedo, N. Mudie, S. Panjikar, J. R. Price, A. Riboldi-Tunnicliffe, R. Rostan, R. Williamson and T. T. Caradoc-Davies, *J. Synchrotron Radiat.*, 2018, **25**, 885–891.